Miner Deposita (2018) 53:417–434
DOI 10.1007/s00126-017-0748-2

ARTICLE

Origin of native copper in the Paraná volcanic province, Brazil, integrating Cu stable isotopes in a multi-analytical approach

Sérgio Benjamin Baggio[1] · **Léo Afraneo Hartmann**[1] · **Marina Lazarov**[2] · **Hans-Joachim Massonne**[3] · **Joachim Opitz**[3] · **Thomas Theye**[3] · **Tillmann Viefhaus**[3]

Received: 2 April 2015 / Accepted: 31 May 2017 / Published online: 29 June 2017

Abstract Different hypotheses exist on the origin of native copper mineralization in the Paraná volcanic province that invoke magmatic, late magmatic, or hydrothermal events. The average copper content in the host basalts is ~200 ppm. Native copper occurs as dendrites in cooling joints, fractures, and cavities within amygdaloidal crusts. Cuprite, tenorite, chrysocolla, malachite, and azurite occur in breccias at the top of the lava flows. Chemical analyses, X-ray diffraction, Raman spectrometry, electron microprobe analyses, LA-ICP-MS, and Cu isotope analyses were used to evaluate the origin of native copper in the volcanic province. Copper contents in magnetite of the host basalt are close to 1 wt.%, whereas clinopyroxene contains up to 0.04 wt.% Cu. Cretaceous hydrothermal alteration of magnetite and clinopyroxene released copper to generate hydrothermal copper mineralization. The isotopic composition of the native copper in the Paraná volcanic province varies from −0.9‰ in the southeastern portion (Rio Grande do Sul state) to 1.9‰ in the central portion (Paraná state) of the province. This study supports a hydrothermal origin followed by supergene enrichment for native copper in the Paraná volcanic province.

Editorial handling: F. Melcher

Electronic supplementary material The online version of this article (doi:10.1007/s00126-017-0748-2) contains supplementary material, which is available to authorized users.

✉ Sérgio Benjamin Baggio
sergio.baggio@ufrgs.br

[1] Universidade Federal do Rio Grande do Sul, Porto Alegre, Rio Grande do Sul, Brazil

[2] Leibniz Universität Hannover, Hannover, Germany

[3] Universität Stuttgart, Stuttgart, Germany

Keywords Paraná volcanic province · Native copper · Copper isotopes · Hydrothermal mineralization

Introduction

Native copper forms economically significant deposits in several intraplate basaltic provinces (e.g., Emeishan, China; MI, USA). In the Paraná volcanic province (PVP), native copper occurs widely distributed; however, no economically feasible deposits have been found yet. The PVP copper occurrences have been studied since the beginning of the last century (Hussak 1906), to understand the origin of Cu concentrations. Different origins for the PVP native copper were suggested, including magmatic (Mello 2000), late magmatic (Szubert et al. 1979), and hydrothermal remobilization (Tazaki et al. 1988; Pinto et al. 2011b; Arena et al. 2014). Here, native copper from a number of localities in the PVP (Fig. 1) was investigated using various analytical techniques: (1) X-ray diffraction (XRD) and Raman spectrometry to identify copper minerals; (2) electron probe microanalysis (EPMA) to determine the major element composition of minerals; (3) laser ablation-inductively coupled plasma-mass spectrometry (LA-ICP-MS) to measure trace element concentrations; and (4) multi-collector ICP-MS to determine copper isotope compositions. The Cu isotope compositions are considered essential to distinguish high-temperature from low-temperature native copper (Larson et al. 2003; Seo et al. 2007; Mathur et al. 2009, 2012). Our integrated analytical approach supports a hydrothermal origin for the copper mineralization, followed by supergene enrichment.

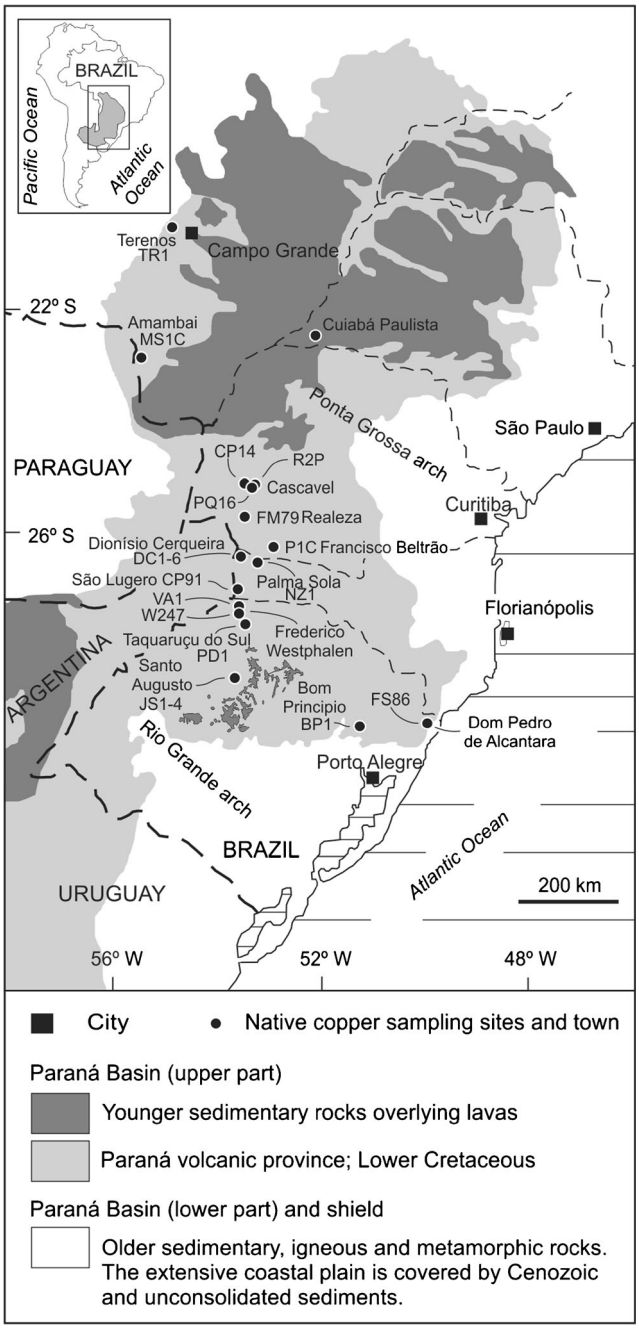

Fig. 1 Geological map of southeastern South America (modified from Peate et al. 1992), highlighting the Paraná volcanic province

Geology

The PVP is one of the largest igneous provinces on land (Bellieni et al. 1984; Hartmann et al. 2010), covering an area of 917,000 km^2 (Frank et al. 2009) in southeastern South America, mainly Brazil but including portions of Uruguay, Argentina, and Paraguay (Fig. 1). The volumes of lava flows, sills, and dikes are around 450,000 and 112,000 km^3, respectively. The Etendeka basalts in Namibia, Africa, were connected to the Paraná volcanic province before the opening of the South Atlantic Ocean (Bellieni et al. 1984). The lava flows of the PVP are predominantly tholeiitic basalts (>90 vol.%) extruded in the Lower Cretaceous. However, basaltic andesite, dacite, rhyodacite, and andesite also occur. Rhyolitic flows are present in the southern portion of the province near the top of the volcanic pile along the Brazilian continental margin (Melfi et al. 1988) and in the Etendeka (Peate 1997). In Brazil, PVP rocks belong to the Serra Geral Group (Wildner et al. 2009), named Serra Geral eruptives by White (1908) and Serra Geral Formation by Gordon (1947). The average U-Pb age of the PVP is between 130 and 135 Ma (Pinto et al. 2011a; Janasi et al. 2011). The thickness of the volcanic pile is associated with the subsidence of the Paraná Basin. In Cuiabá Paulista (Fig. 1), the volcanic pile reaches the highest known thickness (1723 m) equivalent to the depocenter of the PVP—and becomes thinner to the south, reaching 50 m along the Brazil–Argentina border (Almeida 1986). According to Peate et al. (1999), the thickness of single flows varies from 5 to 80 m; the average thickness of individual flows is about 20 m.

The geochemical subdivision of the PVP is based on the TiO_2 content of basalt (Bellieni et al. 1984; Mantovani et al. 1985). In the southern portion, low-Ti basalt (TiO_2 < 2 wt.%) predominates, whereas in the northern part high-Ti basalt (TiO_2 > 2%) are more abundant. These two basalt types were reassessed by Peate et al. (1992), who proposed a new classification based on major and trace elements and specific ratios of elements. The low-Ti group was subdivided into the Gramado, Esmeralda, and Ribeira magma types, and the high-Ti group into the Urubici, Pitanga, and Paranapanema magma types. The study by Nakamura et al. (2003) added an intermediate-Ti type to this new classification. Paranapanema and Ribeira magma types belong to the intermediate-Ti type. The Gramado and Esmeralda are of the low-Ti type, the Pitanga and Urubici of the high-Ti type.

According to Arena et al. (2014), the average copper content in the PVP is 177 ppm. The intermediate-Ti magma types commonly display the highest contents of copper in the province. In particular, the Paranapanema magma type hosts the most abundant occurrences of native copper. Some occurrences of native copper, cuprite, tenorite, chrysocolla, malachite, and azurite in the PVP have been described from hydrothermal breccias at the top of Paranapanema magma type flows. In addition, similar occurrences are found in Pitanga and Gramado magma type flows.

A pioneering study of native copper in the PVP was undertaken by Szubert et al. (1979). These authors proposed that some of the copper occurrences were late magmatic (dendritic shape copper in cooling joints), but others were supergene (copper filling amygdules in basaltic

crusts). Tazaki et al. (1988) alternatively suggested that the Cu mineralization was associated with hydrothermal alteration at a low temperature. These authors pointed to the presence of small amounts of copper in titano-magnetite. The existence of copper in the Vista Alegre region, near the town of Frederico Westphalen (Rio Grande do Sul state), encouraged Costa (1982) to use geophysical methods in the search for native copper. His study yielded negative correlation of induced polarization (IP) anomalies with the magnetite content of basaltic rocks. The study by Pinto et al. (2011b) suggested a hydrothermal origin of native copper with supergene enrichment in the Vista Alegre region based on the H1, H2, and H3 hydrothermal events (Hartmann 2008; Hartmann et al. 2012a, 2012b). These authors proposed that hydrothermal alteration of opaque minerals and pyroxene resulted in the release of copper to form native copper. During the H1 event, amygdules and cooling fractures were filled with zeolite, smectite, and native copper. H2 occurred afterwards by injection of fluidized sand into the basalt. Continued alteration in H3 caused alteration of the basalt into clay minerals and zeolites.

Sampling

Each sample pair consists of the host basalt and associated native copper mineralization. Sample pairs were collected over an extended area of the PVP from 15 occurrences, listed in the Electronic Supplementary Material (ESM 1) and shown in Fig. 1. In Rio Grande do Sul state, dendritic native copper on the surface of cooling joints is found in three quarries: (1) quarry 86, in the town of Dom Pedro de Alcântara; (2) Brasília-Guaíba quarry, in the town of Bom Princípio; and (3) David Basso quarry, in the town of Taquaruçu do Sul (Fig. 2a). In the Santo Augusto region, massive pockets of native copper occur in hydrothermal breccias (Fig. 2b), which contain cuprite, tenorite, chrysocolla, malachite, and azurite, resembling those in the Vista Alegre district (Pinto et al. 2011b).

In Santa Catarina state, the host basalt and dendritic crystals of native copper on a fracture surface were collected at São Ludgero (drill core at 92 m depth). In the Rebelatto quarry (Fig. 2c), in Palma Sola town, a large amount of native copper occurs as blades and dendrites along cooling joints of basalt (Fig. 2d). A native copper occurrence near the town of Dionísio Cerqueira was also sampled. In Paraná state, several occurrences of native copper are known. In the town of Francisco Beltrão, dendritic native copper is found along the cooling joints in two quarries (Petrocon and Dalba). In the Quati quarry (Fig. 2e), massive native copper, in spatial association with zeolite and calcite, fills the central part of cavities

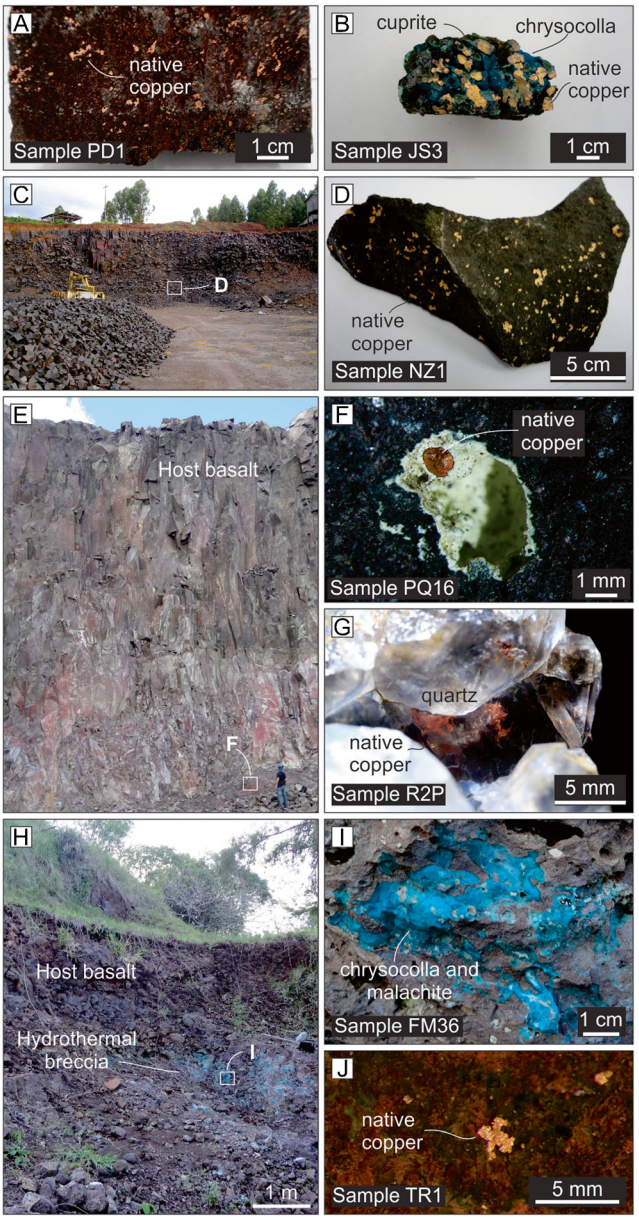

Fig. 2 Field photos of native copper mineralization in the Paraná volcanic province. **a** Dendritic native copper at the surface of cooling joints. Sample PD1 from David Basso quarry, Taquaruçu do Sul, Rio Grande do Sul. **b** Massive native copper with cuprite, tenorite, chrysocolla, and malachite (sample JS3) from Santo Augusto, Rio Grande do Sul. The mineralization occurs in a hydrothermal breccia. **c** Mining front in the Rebelato quarry, in Palma Sola, Santa Catarina, indicating the collection area (sample NZ1). **d** Detail of white square in (**c**). Native copper in thin blades and dendrites at the surface of cooling joints in basalt. **e** Basalt face in the Quati quarry in Francisco Beltrão, Paraná. **f** Detail of (**e**) showing the mineralization of native copper filling the central portion of a cavity in association with zeolites (Sample PQ16). **g** Sample R2P from the Quati quarry with native copper in dendritic shape associated with crystals of quartz. **h** Outcrop in Linha Capanema, Realeza, Paraná, showing the intense blue and green association of malachite and chrysocolla. **i** Detail of (**h**) showing chrysocolla and malachite cementing the hydrothermal breccia. The copper mineralization is also filling the cavities (amygdaloidal crust) of the fragmented basalt

(Fig. 2f), and also occurs as dendrites in the basal portion of quartz-filled cavities (Fig. 2g). However, the main mineralization in Paraná state is at Linha Capanema, in the town of Realeza (Fig. 2h). There, the hydrothermal breccias contain native copper, cuprite, chrysocolla, and malachite (Fig. 2i). In the northwestern portion of the PVP, in Mato Grosso do Sul state, native copper was observed on a fracture surface of a drill core at 10 m depth at Jaguaretê, in the area of Amambai. Very fine dendrites were sampled in the Santo Onofre quarry at Terenos (Fig. 2j) near the city of Campo Grande.

Analytical methods

Polished thin sections of host basalts were used for petrography. Thin sections of 40–50 μm in thickness were prepared for LA-ICP-MS analyses. Selected crystals of native copper and copper minerals were embedded in epoxy mounts, 2.5 cm in diameter, and polished for Raman spectroscopy, EPMA, backscattered electron image and Cu isotope analyses. The analytical work was performed at Universidade Federal do Rio Grande do Sul, Brazil (petrography and XRD), Institut für Mineralogie und Kristallchemie, Universität Stuttgart, Germany (XRD, Raman spectrometry, LA-ICP-MS and EPMA), Institut für Mineralogie, Universität Hannover, Germany (multi-collector ICP-MS), and ACME Analytical Laboratories, Vancouver, Canada (whole-rock major and trace elements).

For whole-rock major element analyses, 0.1-g aliquot was molten in lithium metaborate/tetraborate and subsequently digested in nitric acid. Loss on ignition (LOI) was obtained from the mass difference after heating at 1000 °C. Trace elements were determined by ICP-MS, following the same melting procedure for the major elements, in an 0.5-g aliquot that was digested in aqua regia.

Some copper minerals such as cuprite and malachite were initially identified using a Bruker AXS D8 Advance X-ray diffractometer. Further identification of copper minerals was performed using an Olympus BX51 microscope coupled with a Raman spectrometer (Horiba Xplora) at a wavelength of either 532 or 638 nm, a power of 0.25 to 25 mW and spectral range of 70 and 4000 cm^{-1}. Spectra were obtained by collecting 5 to 100 scans, each with 10-s exposure time, depending on the laser power and the composition of the sample. A Cameca SX100 EPMA was used for wavelength-dispersive-spectroscopy (WDS) analyses of native copper and for backscattered electron images. Experimental conditions were 15 kV, 50 nA, and spot diameter of 1 to 2 μm. In particular, the WDS analyses were used to characterize spots on which the LA-ICP-MS analyses were subsequently carried out. Reference materials and detection limits, as quoted by the Cameca operating software, are summarized in ESM 2.

Trace element concentrations in minerals of the host basalt were determined by ICP-MS analyses with an AGILENT 7700 spectrometer after laser ablation with a CETAC LSX-213 laser system. The diameter of the ablated spots was 50 μm. The laser energy was set to 10% of the maximum (100% = 4 mJ at a spot diameter of 150 μm), at a frequency of 20 Hz. A mixed helium and argon gas flow with 300 and 800 ml/min, respectively, served as carrier of the ablated material. Reference materials were DLH7 and DLH8 from P&H Developments Ltd., and a NIST (National Institute of Standards and Technology, USA) 612 glass. The validity of the calibration, data evaluation, and reproducibility were checked with the reference materials Diorite (DRN) and Zinnwaldite (ZW-C) from Service d'Analyses des Roches et des Mineraux (SARM) du Centre National de la Recherche Scientifique (CNRS). Lithium borate glass disks of both were prepared using 0.6 g of powder of these reference materials and 3.6 g of lithium borate.

The data acquisition was performed using the Agilent Mass Hunter software (version B.01.01). Each analysis comprised the acquisition of the individual background ion intensities for roughly 15 s (gas-blank) followed by the acquisition of the ion intensities on laser irradiation of the sample spot for roughly 40 s. In the offline data evaluation, the analytical signal of each ion was corrected by the subtraction of the corresponding averaged background intensity. Within a selected appropriate interval of the ablation time profile, after each mass cycle the corrected individual ion intensities were divided by the corrected intensity of the selected isotope of the reference element. These individual quotients were averaged. From these mean values, relative elemental concentrations were calculated from the abundance of the corresponding isotope assuming a natural isotopic distribution and an individual calibration factor which was determined under the same experimental conditions. Absolute elemental concentrations were calculated on the basis of the known absolute elemental concentration of an internal reference element. The software used for calibration and data evaluation was developed by J. Opitz (Massonne et al. 2013).

The following isotopes were monitored: ^{24}Mg, ^{25}Mg, ^{27}Al, ^{29}Si, ^{55}Mn, ^{56}Fe, ^{57}Fe, ^{60}Ni, ^{63}Cu, ^{65}Cu, ^{66}Zn, ^{68}Zn, ^{89}Y, ^{90}Zr, ^{91}Zr, ^{93}Nb, ^{95}Mo, ^{107}Ag, ^{109}Ag, and ^{197}Au. This selection excludes isobaric interferences with isotopes of other elements. In the case of Mg, Fe, Zn, Zr, and Ag, for which two isotopes were analyzed, very similar corresponding individual elemental concentrations were obtained, which shows the absence of significant matrix effects. This is emphasized especially for Fe. No significant interference by $[ArO]^+$ on Fe at m/z 56 was detected. For this reason, the given values are the average of the corresponding individual elemental concentrations. While running the analyses, signals of laser ablation were stable for all minerals.

As mentioned, all elemental concentrations were calculated relative to an internal reference element. Iron was used for magnetite and ilmenite, whereas silicon was used for smectite, clinopyroxene, and plagioclase. The absolute concentration of the internal reference element was previously measured by EPMA (ESMs 3, 4, and 5). As the same mineral target was applied for both EPMA and LA-ICP-MS, the results show that the internal errors for reference and samples were less than 6% (ilmenite), 4% (magnetite and clinopyroxene), and 3% for smectite.

Measurements of copper isotope ratios were performed on a multi-collector ICP-MS Finnigan Neptune instrument, connected to a 194-nm UV, femtosecond-laser-ablation system (Spectra Physics Solstice, USA) at Leibniz Universität Hannover, Germany. Eleven specimens with Cu minerals were selected from samples collected in Rio Grande do Sul (samples FS86, BP1, JS3, JS4, PD1, W247), Santa Catarina (DC6, NZ1), and Paraná (P1C, CP14, R2P). Some of these specimens contained more than one native copper crystal. Samples and reference materials were analyzed in line mode applying a spot size of 35 μm. Laser energy of 0.03 mJ, and laser pulse frequency of 2.0–4.5 Hz were used. Instrumental mass bias discrimination was corrected using the $^{62}Ni/^{60}Ni$ ratio of the Ni NIST SRM-986 reference solution, which was monitored simultaneously with the laser ablation signal of Cu isotopes. The solid Cu NIST SRM976 metal reference material was used for the reference sample bracketing. Usually three sample measurements were bracketed by reference material measurements. Results are reported as $\delta^{65}Cu$ in permil (‰) as follows: $\delta^{65}Cu = [(((^{65}Cu/^{63}Cu)_{sample} / (^{65}Cu/^{63}Cu)_{NIST\ SRM976})-1] \times 1000$. Internal error for reference material and samples were better than 0.05‰ (2 SD) and the overall precision of reference material measurements was better than 0.08‰ (2 SD), as reported by Lazarov and Horn (2015). Femtosecond laser ablation has been considered one of the most accurate for isotope studies (Lazarov and Horn 2015; Horn et al. 2006; Horn and von Blanckenburg 2007). The method showed no isotopic fractionation even when the analyses were conducted without matrix match or when using different protocols (spots, lines, and raster) between samples and calibration standards. Additional details of instrumental and measurement settings can be found in Oeser et al. (2014) and Lazarov and Horn (2015).

Results

Petrography, XRD, and Raman

The basalt host rock samples of the PVP are holocrystalline and microporphyritic and contain plagioclase, clinopyroxene, and opaque minerals in transmitted light (e.g., magnetite and ilmenite) as phenocrysts from 0.6 to 1.5 mm across. Small crystals of the same minerals form an intergranular matrix (Fig. 3a). In some cases, phenocrysts of plagioclase and opaque minerals display a glomeroporphyric texture. The average mineralogical composition of the host rocks to native copper in the PVP is 45% plagioclase, 30% clinopyroxene, 12% opaque minerals, 8% microcrystalline matrix, 5% secondary clay minerals, and traces of apatite.

Crystals of plagioclase are subhedral to euhedral and exhibit random distribution and sharply defined rims (Fig. 3b). A few crystals display optical zoning. No alteration of plagioclase was detected. Magnetite and ilmenite are euhedral to anhedral and frequently form poikilitic aggregates. Ilmenite usually occurs as exsolution lamellae in magnetite. In several crystals, the opaque minerals show corroded rims (Fig. 3c). In particular, a reddish halo containing hematite can be observed (Fig. 3d). Clinopyroxene is commonly subhedral to anhedral, usually fractured and little altered (Fig. 3e). The grain edges are well defined and straight, mainly near plagioclase.

The microcrystalline matrix, which occupies the interstitial space between phenocrysts (Fig. 3f), contains tiny crystals of clinopyroxene from 0.05 to 0.1 mm, K-feldspar (≤0.1 mm) and quartz (≤0.1 mm). Acicular apatite is an accessory mineral.

Clay minerals in the host basalt comprise smectite and, occasionally, celadonite. The occurrence of native copper in cavities or in cooling joints of the host basalt is spatially associated with clay minerals, zeolite, and calcite.

Powder-XRD analyses (Fig. 4) of three selected samples (JS3a, JS3b, and JS3c from Santo Augusto region, Rio Grande do Sul) indicate cuprite and malachite. XRD spectra also indicate amorphous, non-crystalline materials, which were analyzed by Raman spectroscopy. For the Raman analyses, five epoxy mounts were prepared from samples JS2, JS3, JS4, R2P, and VA1. These mounts contain native copper from Santo Augusto, Cascavel, and Vista Alegre. Six copper minerals were characterized: native copper, cuprite, tenorite, chrysocolla, and malachite. Azurite peaks were identified in association with chrysocolla peaks. The native copper shows no Raman signal, but a broad peak at frequencies between 2000 and 3100 cm^{-1} (Fig. 5a, b). Cuprite occurs together with native copper, representing the most frequent copper mineral association in the PVP, and displays unambiguous Raman spectra (Fig. 5c, d). Tenorite is not as common as cuprite but occurs together with cuprite (Fig. 5e, f). Chrysocolla and malachite can be detected from the Raman spectra (Fig. 5g–j), in which quartz, magnetite, hematite, and zeolite (heulandite) were also identified. Silver was also detected in the Raman spectra at 611.5, 523.9, 207.7, 140.1, 89.1, and 52.5 cm^{-1}. It occurs in spatial association with the native copper and other copper minerals in several places of the PVP (Fig. 6).

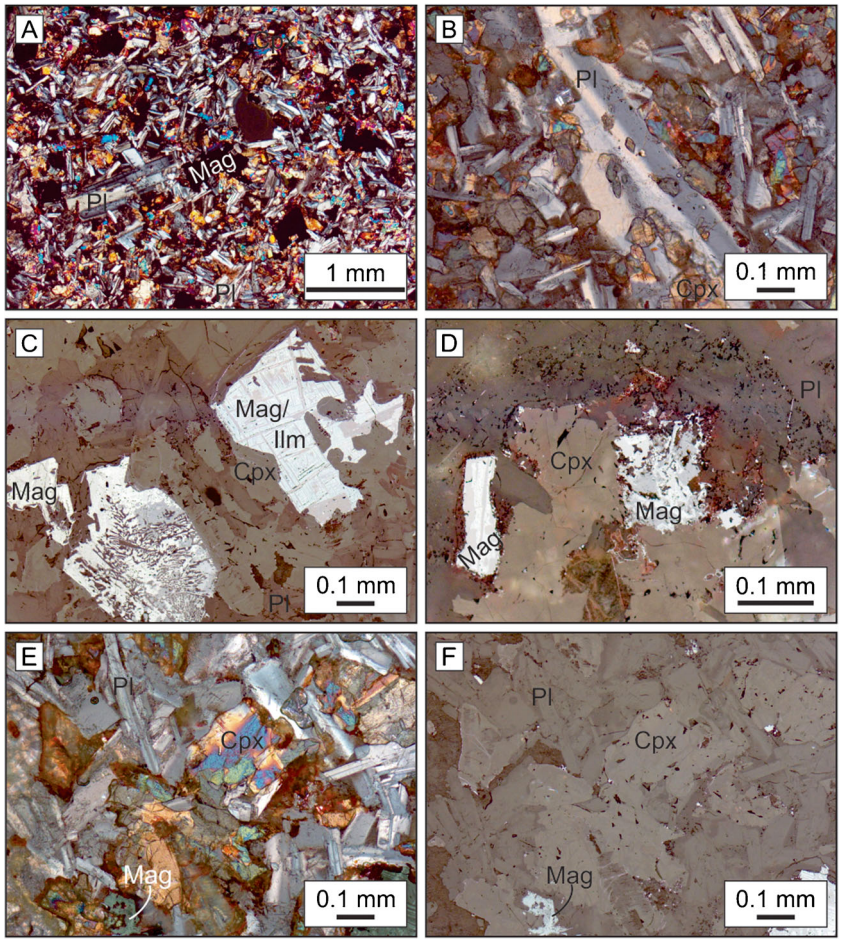

Fig. 3 Photomicrographs of basalts hosting native copper from the Paraná volcanic province. *Cpx* clinopyroxene, *Ilm* ilmenite, *Mag* magnetite, *Pl* plagioclase. **a** Intergranular texture of small crystals of plagioclase, clinopyroxene, and opaque minerals. Glomeroporphyritic texture with phenocrysts of plagioclase and opaque minerals. Cross-polarized light (sample PD1). **b** Phenocrysts of plagioclase associated with smaller crystals of clinopyroxene and plagioclase. Cross-polarized light (sample W247). **c** Microphenocrysts of magnetite partly altered to clay minerals (*left*), reflected light (sample PD1). **d** Magnetite with reddish halo of hematite (*center* and *left*), reflected light (sample PD1). **e**, **f** Sample NZ1 with clinopyroxene and plagioclase crystals, microcrystalline matrix in the interstitial space between the phenocrysts, and presence of opaque minerals in the matrix. **e** Cross-polarized light. **f** Reflected light

Whole-rock major and trace element composition

Major and trace element contents of the volcanic rocks ($n = 13$) are presented in Table 1. According to the classification of Le Bas et al. (1986), the rocks are basalt and basaltic andesite, the SiO_2 contents of which are between 49.5 and 50.9 wt.% for basalt and 53.0 wt.% for basaltic andesite (Fig. 7a). The contents of $Na_2O + K_2O$ are between 2.8 and 4.5 wt.% for basalts and 4.8 wt.% for basaltic andesite. The native copper mineralization occurs in all analyzed magma types (Fig. 7b). The whole-rock (WR) trace element compositions show the lowest contents of copper in the southwestern portion of the PVP, between 83 ppm at Dom Pedro de Alcântara, RS, and 98 ppm at Bom Princípio, RS. The highest contents are between

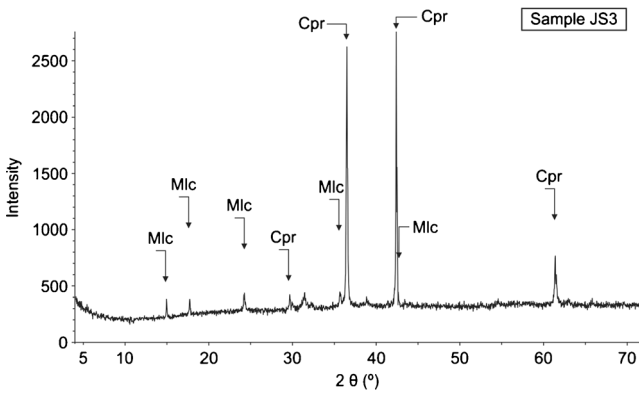

Fig. 4 X-ray diffraction pattern of sample JS3 from Santo Augusto, Rio Grande do Sul. *Cpr* cuprite, *Mlc* malachite

Fig. 5 Photomicrographs (plane polarized light) and Raman spectra of copper minerals. *Ccl* chrysocolla, *Cpr* cuprite, *Mlc* malachite, *Tnr* tenorite. **a** Sample JS3 with location of the Raman spot. **b** Raman spectra of indicated spot in (**a**) showing broad peaks at frequencies between 2000 and 3100 cm^{-1} that identify the presence of native copper. **c** Sample VA1 with location of the Raman spot. **d** Raman spectra of indicated spot in (**c**) showing the identification of cuprite. **e** Sample JS2 with location of the Raman spot. **f** Raman spectra of indicated spot in (**e**) displaying tenorite peaks. **g** Sample JS2 with location of the Raman spot. **h** Raman spectra of indicated spot in (**g**) showing the identification of chrysocolla peaks. **i** Sample JS2 with location of the Raman spot. **j** Raman spectra of indicated spot in (**i**) presenting malachite peaks

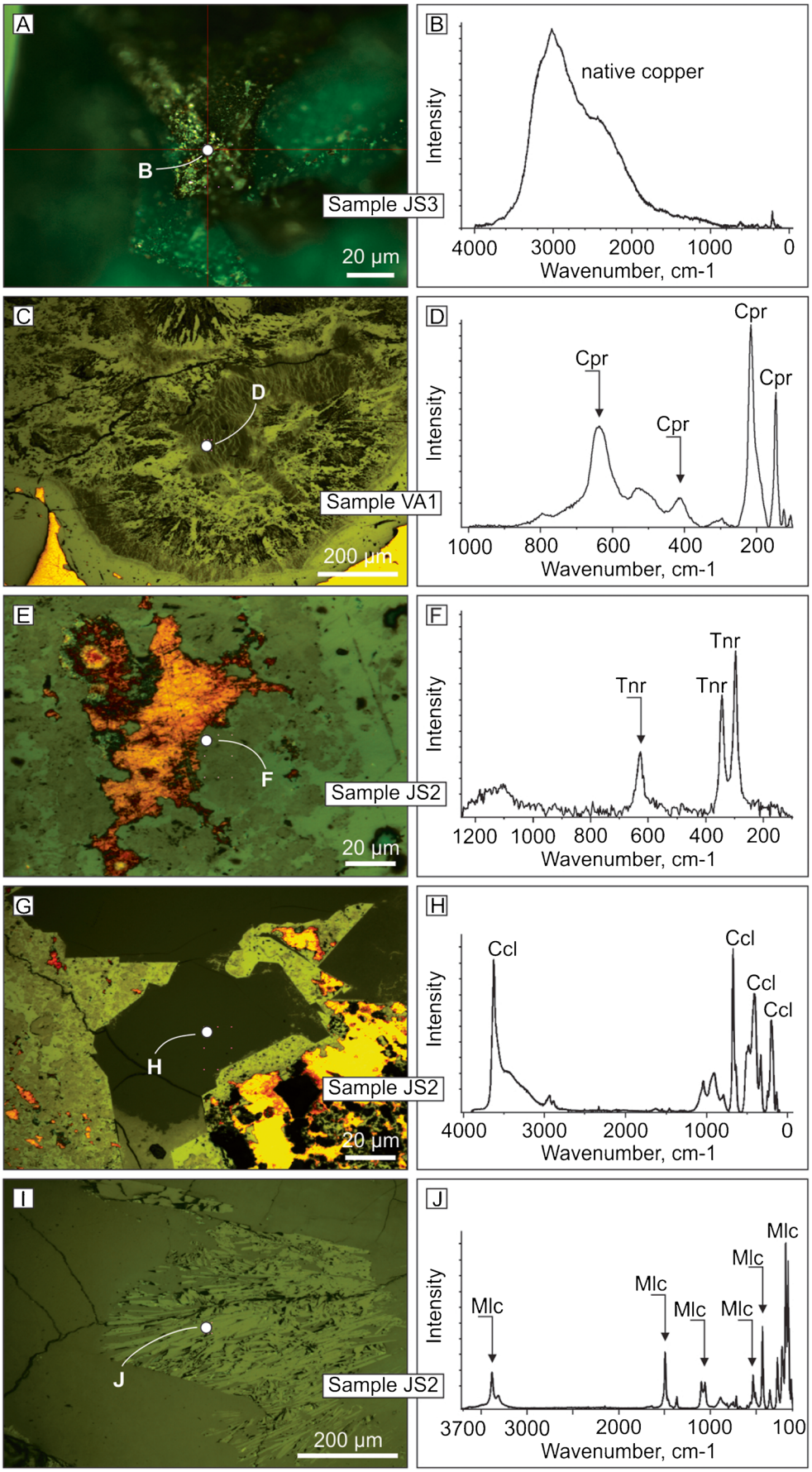
A
B
Sample JS3
20 μm
B
native copper
Intensity
4000 3000 2000 1000 0
Wavenumber, cm-1
C
D
Sample VA1
200 μm
D
Cpr
Cpr
Cpr
Cpr
Intensity
1000 800 600 400 200
Wavenumber, cm-1
E
F
Sample JS2
20 μm
F
Tnr
Tnr
Tnr
Intensity
1200 1000 800 600 400 200
Wavenumber, cm-1
G
H
Sample JS2
20 μm
H
Ccl
Ccl
Ccl
Ccl
Intensity
4000 3000 2000 1000 0
Wavenumber, cm-1
I
J
Sample JS2
200 μm
J
Mlc
Mlc
Mlc
Mlc
Mlc
Intensity
3700 3000 2000 1000 100
Wavenumber, cm-1

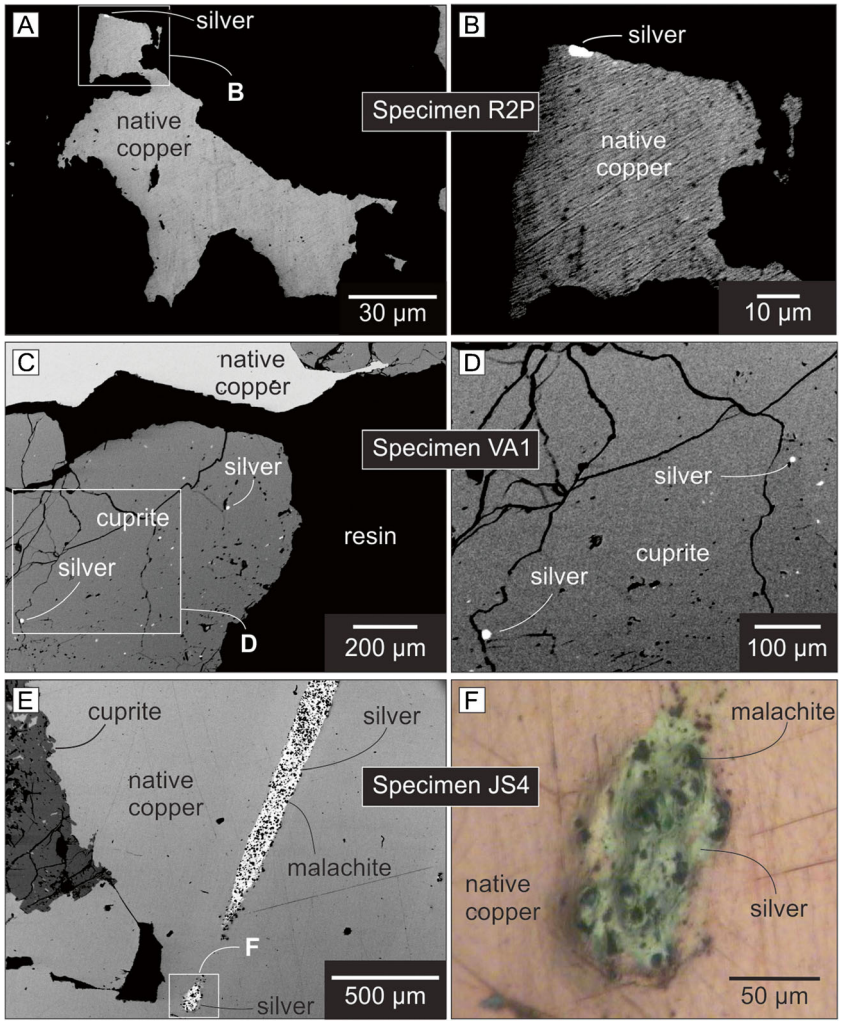

Fig. 6 Backscattered electron images of silver inclusions in copper crystals. **a** Silver inclusion in native copper crystal of specimen R2P from Dalba quarry, Francisco Beltrão, Paraná state. **b** Detail of white square in (**a**) showing the spatial relationship between silver and copper. **c** Cuprite associated with native copper. Silver inclusions occur in the cuprite crystal of specimen VA1 from Vista Alegre mining district, Vista Alegre, Rio Grande do Sul state. **d** Detail of (**c**) showing the microsilver inclusions disseminated in the cuprite. **e** Native copper associated with cuprite, silver, and malachite. Silver vein and malachite occur together in the native copper crystal of specimen JS4 from Santo Augusto, Rio Grande do Sul state. **f** Detail of (**e**) showing the spatial relationship between malachite (*black dots*), silver, and native copper (plane polarized light photomicrograph)

292 ppm at Dionísio Cerqueira, SC, and 324 ppm at Frederico Westphalen, RS. The average Cu content of our samples is 207 ppm ($n = 16$), slightly above that established by Arena et al. (2014) for the PVP. In sample DC6, Cu reaches 1115 ppm, a value that likely represents a nugget effect because the sample contains small native copper crystals along joints.

According to Hartmann et al. (2010), Duarte et al. (2009, 2011), and Rosenstengel and Hartmann (2012), LOI is an important geochemical parameter in the PVP hydrothermal environment because it is a proxy for the hydrothermal alteration. Copper versus LOI contents shows large regional variation. The WR copper contents display a positive correlation with MnO and Fe_2O_3 (Fig. 7c). The correlation of copper with trace elements is not significant except for the REE that exhibit positive correlation with Cu, in particular the heavy REE (Fig. 7d).

Mineral chemistry

Three-hundred and five EPMA analyses of native copper show that this mineral is virtually pure Cu (Fig. 8), other elements amounting to less than 0.3 wt%. The contents of Sn, Ca, Co, Ni, U, and Al are below the detection limit of the EPMA (see ESM 2). Silicon was measured to monitor the presence of silicate inclusions. Small, but significant, Si contents coincide with Fe concentrations in sample TR1. This coincidence is due to microinclusions of Fe-bearing silicate in native copper. Sulfur contents were close to, or even below, the detection limit (113 ppm) of the EPMA.

The silver content in native copper is also mostly below the detection limit (440 ppm). Where silver inclusions were observed (samples R2P, VA1, and JS4), there is a wide variation of silver contents, up to 0.28 wt.% (sample VA1), in the native copper. These higher Ag contents may be related to microinclusions of native silver. Gold is below the detection limit (1242 ppm), in agreement with the general absence of gold inclusions in spatial association with native copper in the PVP.

The results for the trace elements of magnetite, ilmenite, smectite, clinopyroxene, and plagioclase using LA-ICP-MS are listed in ESMs 3, 4, 5 and depicted in Fig. 9a–d. Emphasis is placed on Cu contents. Magnetite shows an

Table 1 Chemical analyses of host volcanic rock (native copper mineralization). Paraná volcanic province

Sample	FS86	BP1	JS1–4	PD1	CP91	DC2	DC6	NZ1	P1C	CP14	PQ16	MS1C	TR1
SiO_2	50.26	50.74	50.38	50.59	49.54	50.52	50.39	50.53	49.95	50.86	50.16	53.00	49.62
TiO_2	1.60	1.03	2.20	2.27	2.21	2.23	2.31	2.36	2.20	2.41	2.34	2.89	3.76
Al_2O_3	16.08	14.79	12.77	12.50	13.24	12.79	12.45	12.54	13.07	12.64	12.68	12.05	12.61
Fe_2O_3	10.82	10.89	15.35	15.83	14.67	15.31	16.21	16.15	14.30	15.51	15.52	13.95	15.20
MgO	4.79	7.85	4.91	4.80	5.64	5.01	4.83	4.79	4.73	4.58	4.74	3.86	4.38
CaO	10.36	10.40	8.71	8.74	9.90	8.95	8.78	8.68	8.84	8.84	8.84	5.50	8.38
Na_2O	2.28	1.89	2.39	2.44	2.41	2.44	2.39	2.49	2.26	2.50	2.44	2.44	2.66
K_2O	1.37	0.92	1.63	1.23	1.08	1.16	1.19	1.15	2.24	1.11	1.09	2.32	1.48
P_2O_5	0.28	0.13	0.25	0.26	0.25	0.25	0.26	0.27	0.27	0.28	0.26	0.78	0.39
MnO	0.15	0.16	0.20	0.23	0.20	0.22	0.22	0.24	0.21	0.21	0.22	0.19	0.21
Cr_2O_3	0.018	0.053	0.012	0.008	0.016	0.009	0.009	0.012	0.016	0.007	0.009	0.005	0.004
LOI	1.7	0.9	0.9	0.8	0.5	0.8	0.6	0.5	1.6	0.8	1.4	2.7	1
Total	99.75	99.75	99.72	99.72	99.69	99.71	99.62	99.71	99.72	99.73	99.72	99.65	99.67
Au	–	3.0	4.0	5.3	1.1	4.1	1.2	7.2	2.4	–	–	4.7	–
Ba	349	224	316	306	320	284	287	299	310	313	311	682	451
Ce	48.9	30.5	46,7	47.7	48.3	45	45.7	48.5	47.6	50.1	50	110.2	70.2
Co	33.9	42.2	42.6	40.6	42.2	41.4	39.2	41.5	37.7	42.6	42.9	29.2	39.1
Cs	0.9	0.4	0.4	0.3	-	0.3	0.2	-	0.5	0.3	0.3	0.4	0.3
Cu	83.0	97.7	173.2	272.7	258.6	292.2	1114.7	176.5	189.0	263.8	149.3	212.2	103.6
Dy	4.98	3.37	6.58	6.57	5.29	6.48	6.52	6.64	4.76	6.52	6.96	9.92	6.64
Er	2.62	2.03	3.96	3.75	2.93	3.68	3.89	3.94	2.71	3.58	3.62	4.83	3.52
Eu	1.52	1.06	1.78	1.80	1.78	1.81	1.78	1.87	1.65	1.76	1.86	3.41	2.48
Ga	19.2	15.2	17.6	18.9	20.2	18.9	18.1	20.1	18.6	18.6	19.3	22.0	21.1
Gd	5.22	3.62	6.48	6.47	5.53	6.33	6.5	6.77	5.45	6.92	6.85	10.87	7.30
Hf	4.4	2.8	4.5	4.5	4.1	4.7	4.8	4.7	3.6	5.1	4.8	8.9	6.3
Ho	0.99	0.70	1.45	1.31	1.05	1.38	1.33	1.39	0.94	1.34	1.35	1.78	1.30
La	23.5	15.3	22.5	21.6	23.4	21.3	22.4	22.7	21.5	22.3	22.2	52.9	31.0
Lu	0.35	0.28	0.51	0.55	0.37	0.52	0.52	0.53	0.38	0.52	0.51	0.66	0.43
Mo	0.4	0.2	0.9	0.6	0.3	0.3	2.1	1.5	0.5	0.5	0.4	1.5	1.3
Nb	18.4	7.4	13.4	13.1	13.9	13.1	13.3	13.6	12.9	13.8	14.2	29.4	21.5
Nd	25.6	14.3	25.3	25.3	25.2	25.5	25.8	26.0	23.6	28.2	24.7	55	36.8
Ni	64	136	57	48	67	55	56	50	42	29	34	-	37
Pb	2.3	2.1	1.2	1.7	3.2	1.3	1.9	1.5	1.5	1.6	1.9	1.7	1.8
Pr	6.03	3.69	5.94	6.10	5.94	5.82	5.91	6.01	5.70	6.18	6.05	13.5	8.77
Rb	38.3	25.3	54.7	29.0	21.9	23.8	24.0	21.9	81.4	22.8	22.3	51.1	28.3
Sc	33	36	41	40	39	41	41	41	35	39	39	27	31
Sm	5.07	3.22	5.82	5.79	5.37	5.82	5.97	5.97	5.25	5.94	6.11	11.06	7.71
Sr	339.2	221.3	253.3	264.7	382.1	246.8	244.2	244.8	338.7	255.1	262.5	416,4	470.0
Ta	1.1	0.4	0.8	0.9	0.9	0.8	0.9	0.8	0.7	0.9	0.9	1.8	1.3
Tb	0.84	0.62	1.07	1.07	0.91	1.10	1.12	1.11	0.80	1.04	1.05	1.66	1.19
Th	4.3	3.0	2.3	2.4	2.4	2.5	2.2	2.5	2.7	2.8	2.6	6.1	3.1
Tm	0.37	0.30	0.56	0.57	0.43	0.57	0.53	0.55	0.41	0.54	0.57	0.69	0.45
U	0.8	0.6	0.4	0.5	0.4	0.4	0.4	0.4	0.6	0.8	0.7	1.1	0.7
V	257	272	429	445	439	408	424	442	476	474	479	294	466
Y	25.4	19.8	34.8	37.1	26.5	32.4	34.4	34.6	25.9	36.5	35.5	47.5	33.4
Yb	2.24	1.80	3.45	3.21	2.72	3.34	3.46	3.59	2.51	3.46	3.42	4.21	2.85
Zn	47	33	54	76	87	62	73	65	91	69	58	69	66
Zr	164.3	101.1	173.4	163.2	155.6	171.6	177.9	182.4	144.3	175.3	175	347.4	246.7

Provided by ACME Analytical Laboratories Ltd. Oxides in wt.%, trace elements in ppm except Au in ppb; (−) below detection limit (Cs = 0.1, Au = 0.5, Ni = 20). Analyses of whole-rock (WR) samples VA1, FM79, and W247 indicated in the manuscript correspond to sample VVA-12 of Pinto and Hartmann (2011), LC3B of Arena et al. (2014), and VIF11 of Pinto et al. (2011b), respectively

average content of about 1100 ppm (n = 30 spots), with a highly variable distribution from negligible values in sample BP1 (12 ppm) to very high contents in sample PQ16 (>9000 ppm). Four spot measurements on ilmenite from sample PQ16 (ESM 3) indicate that the variability of copper contents is similar to that of magnetite. However, the highest copper content in ilmenite is 3595 ppm, nearly three times smaller than the highest copper content found in magnetite of the same sample. In clinopyroxene (ESM 4), copper contents are smaller than those in magnetite and ilmenite. The average is 97 ppm Cu (n = 28 spots), which varies from values as low as 0.7 ppm to a maximum value of 431 ppm. Plagioclase has Cu contents between 0.02 and 92 ppm. Matrix minerals of the host basalts are usually clinopyroxene, K-feldspar, apatite, and in a few cases quartz. One spot on the matrix material yielded a copper content of 16 ppm (sample FS86).

Some crystals of magnetite and clinopyroxene exhibit slightly corroded rims, whereas magnetite–ilmenite

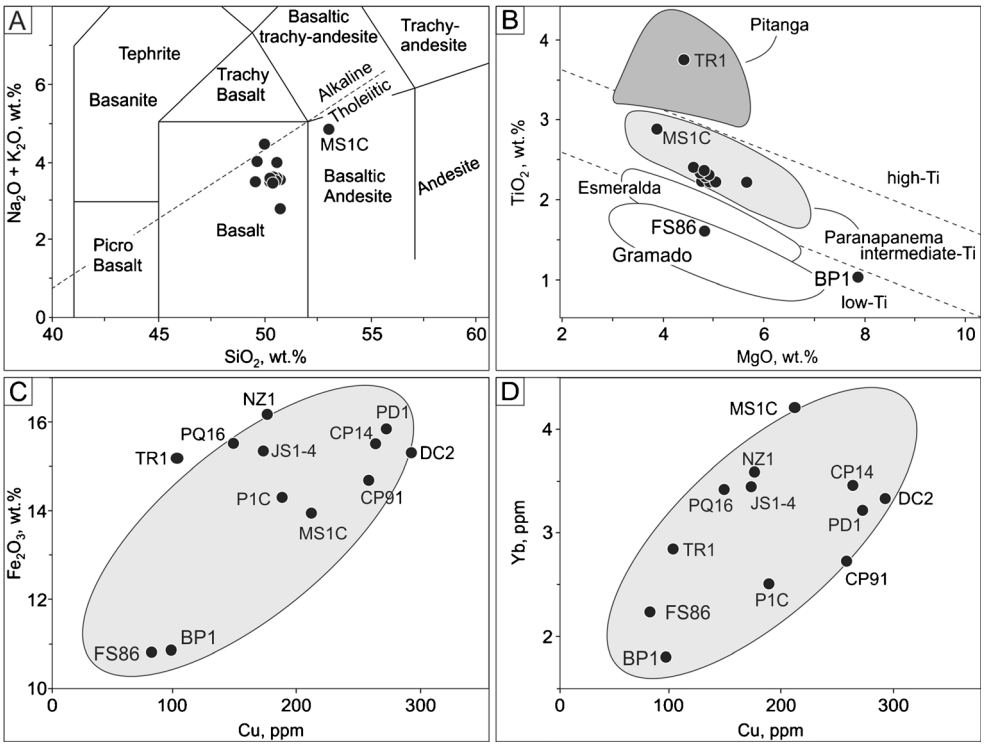

Fig. 7 Classification diagrams of basalts hosting copper from the Paraná volcanic province. **a** Total alkalis–silica (TAS) diagram (after Le Bas et al. 1986). **b** TiO_2 versus MgO diagram, after Peate et al. (1992) and Nakamura et al. (2003). **c** Fe_2O_3 versus Cu diagram showing the contents of copper and iron oxide of the samples and their positive correlation. **d** Yb versus Cu diagram showing a positive correlation

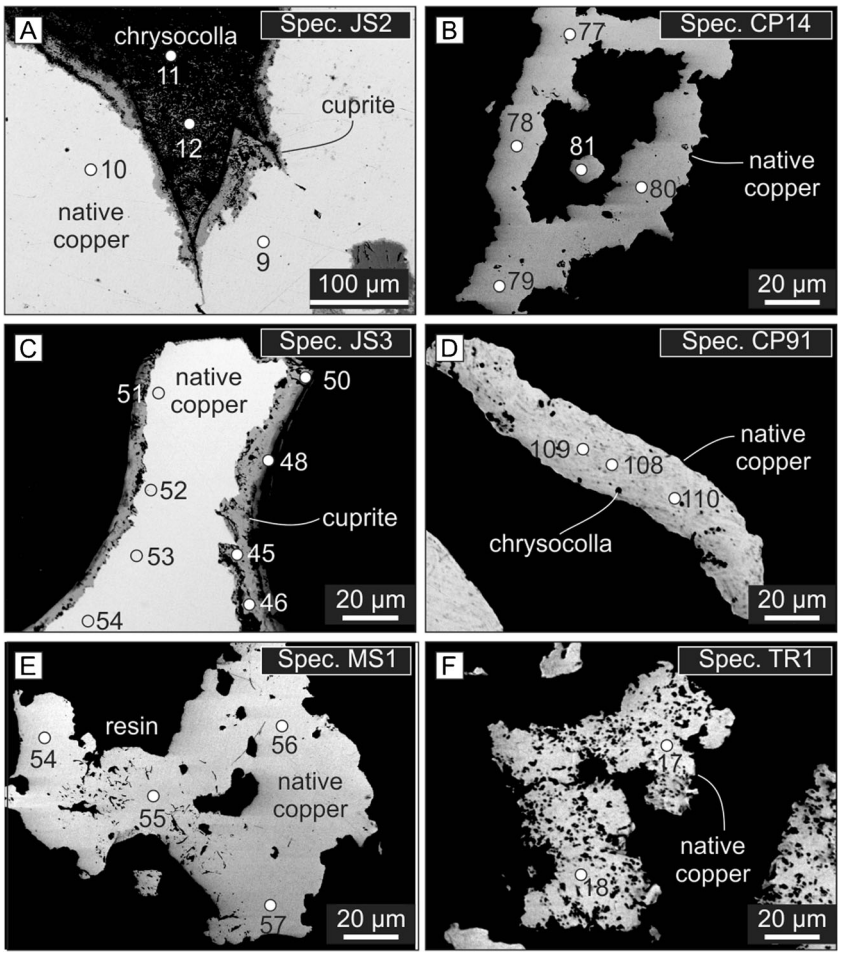

Fig. 8 Backscattered electron images of studied copper minerals. *Numbers* on images indicate the analytical spots of EPMA. **a** Native copper associated with cuprite and chrysocolla (JS2). **b** Dendrite of native copper (CP14). **c** Native copper in the crystal core associated with cuprite in the rim (JS3). **d** Dendrite of native copper associated with chrysocolla (CP91). **e** Dendrite of native copper (MS1). **f** Dendrite of native copper (TR1)

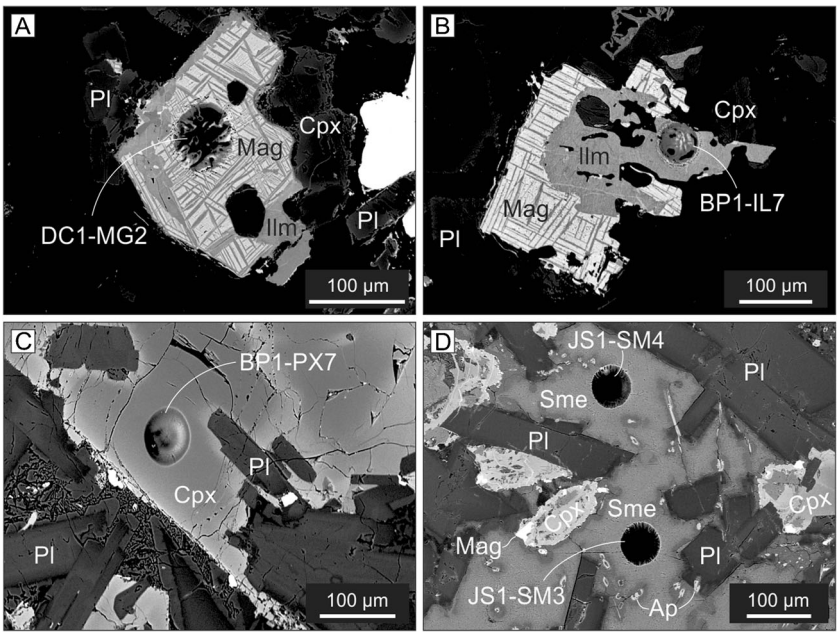

Fig. 9 Backscattered electron images of basalt minerals hosting native copper. *Dark spots* are LA-ICP-MS craters. Sample spot numbers are indicated, e.g., DC1-MG2. *Ap* apatite, *Cpx* clinopyroxene, *Ilm* ilmenite, *Mag* magnetite, *Pl* plagioclase, *Sme* smectite. **a** Magnetite crystal from sample DC1. **b** Mineral association in sample BP1; analyzed ilmenite crystal highlighted. **c** Crystal of analyzed clinopyroxene of sample DC1. **d** Mineral assemblage of sample JS1 with emphasis on two analyses performed on smectite

aggregates display hematite (along the rim) and smectite (Fig. 10a–c). Smectite was observed in all samples of host rocks. Its Cu contents (ESM 5) vary from 1.5 to 500 ppm. Higher contents are considered as a nugget effect from the presence of native copper (Fig. 10d–f) in smectite. These native copper concentrations are found in smectite from highly altered basalt.

The LA-ICP-MS analyses indicate low and variable contents of silver and gold in silicate and oxide minerals of the host basalt. The detection limits for Au and

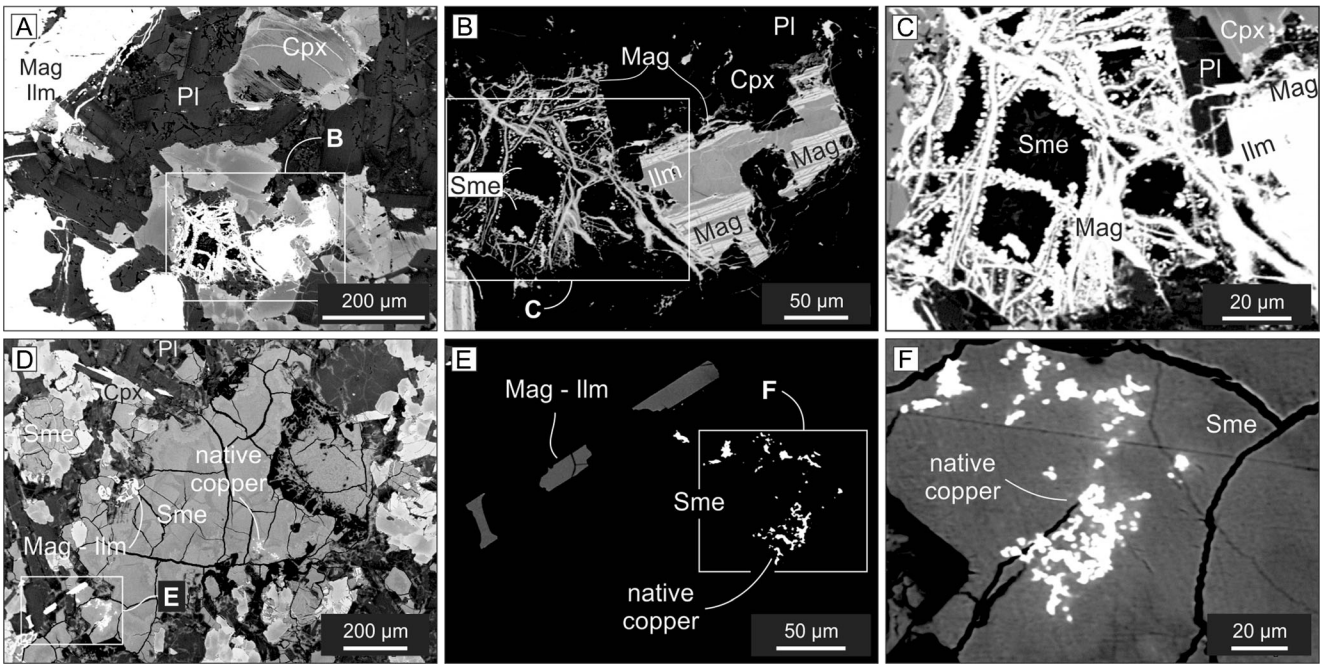

Fig. 10 Backscattered electron images of basalts. *Cpx* clinopyroxene, *Ilm* ilmenite, *Mag* magnetite, *Pl* plagioclase, *Sme* smectite. **a** Spatial relationship of minerals, highlighting areas with alteration in the crystals of magnetite–ilmenite. **b** Detail of the white square highlighted in (**a**). Altered rims of the magnetite and ilmenite crystals. **c** Detail of (**b**). Highlighted presence of smectite in the core of magnetite-ilmenite altered crystals. **d** Contact relationship between crystals of smectite, native copper, magnetite-ilmenite, clinopyroxene, and plagioclase. **e** Detail of (**d**) showing fragments of magnetite-ilmenite and native copper in smectite. **f** Detail of (**e**) showing the concentration of native copper crystals in smectite

Ag are 0.1 ppm. Silver contents are between 0.1 and 1.7 ppm in magnetite and reach 2.7 ppm in ilmenite. In clinopyroxene and smectite, Ag values are up to 1.0 and 1.8 ppm, respectively. The maximum gold content was found in smectite (0.14 ppm) and magnetite (0.12 ppm), whereas in clinopyroxene Au is below the detection limit.

Copper isotopes

Copper isotope ratios in the PVP display three populations (Table 2). The most frequent population has δ^{65}Cu values between −0.20 and 0.71‰ (n = 41). The second population is characterized by δ^{65}Cu values between 1.07 and 1.89‰ (n = 9), with a dominance of δ^{65}Cu values lower than 1.2‰ (n = 6). The third population is characterized by negative δ^{65}Cu values between −0.59 and −0.91‰.

The copper isotopic distribution in the PVP presents a range of values that varies from south to north. Negative δ^{65}Cu values occur in the southern portion of PVP (Rio Grande do Sul) where the greatest regional isotopic variation was observed. Copper occurrences in the southern region show isotope variation ranging from −0.91‰ in Dom Pedro de Alcântara (FS86a) to 1.07‰ in Santo Augusto (JS4c). Samples JS3 and JS4 provided crystals of native copper, cuprite, and chrysocolla. Native copper crystals from both samples show local isotope variations with values between 0.14 and 1.07‰. In the cuprite crystals (JS4b), the isotopic variation was observed from the core (0.16 to 0.21‰) to the rim (0.10 to 0.73‰) while chrysocolla crystals display negative isotope values from −0.27 to −0.34‰.

In the northern portion of Rio Grande do Sul (Taquaruçu do Sul and Frederico Westphalen), a significant variation of Cu isotope ratios was also observed. In the copper crystals of sample W247, the isotopic variation occurs from the core (0.37‰) to the rim (−0.20 to −0.05‰), while in sample PD1, Cu isotope ratios range from 0.70 to 1.18‰.

Towards the north, in the states of Santa Catarina and Paraná, the occurrences of native copper show a range of isotopic variations with positive values. In Santa Catarina, the δ^{65}Cu values range from 0.47 to 1.11‰, while in Paraná state, near the PVP depocenter, the values vary between 0.31 and 1.89‰. This highest value was observed in a centimeter-sized native copper crystal (sample CP14b) from the town of Cascavel. In this locality, millimeter-sized native copper crystals were also collected (CP14a) that present isotopic ratios varying between 0.53

Table 2 Results of Femtosecond-laser ablation Cu isotope measurements - PVP. NIST-SRM 976 Cu standard. Samples listed from south to north (See Fig. 1)

Sample	Type	∂^{65}Cu (‰)	$2\sigma\ \partial^{65}$Cu (‰)
FS86a	Native copper dendrite	−0.91	± 0.05
FS86a		−0.86	± 0.05
FS86a		−0.83	± 0.06
FS86a		−0.88	± 0.05
FS86a		−0.59	± 0.05
FS86b	Native copper dendrite	0.09	± 0.05
FS86b		0.02	± 0.05
BP1	Native copper dendrite	0.37	± 0.05
BP1		0.44	± 0.05
BP1		0.47	± 0.05
JS3a	Native copper massive	0.10	± 0.05
JS3a		0.10	± 0.04
JS3a		0.13	± 0.05
JS3a		0.22	± 0.05
JS3a		0.17	± 0.05
JS3b	Chrysocolla	−0.27	± 0.05
JS3b		−0.34	± 0.05
JS3b		−0.33	± 0.05
JS4a	Native copper massive	0.62	± 0.04
JS4a		0.63	± 0.04
JS4a		0.69	± 0.05
JS4a		0.65	± 0.05
JS4b	Cuprite (rim)	0.12	± 0.04
JS4b		0.10	± 0.04
JS4b		0.73	± 0.05
JS4b		0.32	± 0.04
JS4b	Cuprite (core)	0.16	± 0.04
JS4b		0.21	± 0.04
JS4c	Native copper massive	1.07	± 0.04
PD1a	Native copper dendrite	0.70	± 0.05
PD1a		0.71	± 0.04
PD1b	Native copper dendrite	1.14	± 0.05
PD1b		1.18	± 0.05
W247a	Native copper dendrite (rim)	−0.20	± 0.05
W247a		−0.16	± 0.05
W247a		−0.05	± 0.05
W247b	Native copper dendrite (core)	0.37	± 0.05
DC6	Native copper dendrite	1.09	± 0.04
DC6		1.09	± 0.05
DC6		1.11	± 0.05
NZ1	Native copper dendrite	0.47	± 0.06
NZ1		0.48	± 0.06
NZ1		0.51	± 0.05
P1C	Native copper dendrite (rim)	0.32	± 0.05

Table 2 (continued)

Sample	Type	∂^{65}Cu (‰)	2σ ∂^{65}Cu (‰)
P1C		0.37	± 0.05
P1C		0.37	± 0.05
P1C		0.42	± 0.05
P1C		0.31	± 0.04
P1C	Native copper dendrite (core)	0.36	± 0.04
P1C		0.43	± 0.05
P1C		0.41	± 0.04
P1C		0.38	± 0.04
R2P	Native copper dendrite	0.55	± 0.04
R2P	with quartz	0.56	± 0.04
R2P		0.51	± 0.04
R2P		0.64	± 0.04
R2P		0.61	± 0.04
CP14a	Native copper blades (mm)	0.57	± 0.04
CP14a		0.62	± 0.05
CP14a		0.53	± 0.04
CP14a		0.55	± 0.05
CP14b	Native copper dendrite (cm)	1.50	± 0.05
CP14b		1.51	± 0.05
CP14b		1.89	± 0.05

and 0.62‰. These δ^{65}Cu ratios confirm the local and regional isotope variation in the PVP.

Discussion

Studies on the origin of native copper deposits have resulted in genetic models for a wide variety of deposits hosted in mafic and ultramafic igneous, sedimentary rocks, and in sulfide deposits (Cornwall 1956; Dekov et al. 2013). In the PVP, three genetic models have been proposed for native copper, magmatic, late magmatic, and hydrothermal. The magmatic model suggested by Mello (2000) explains that native copper mineralization at the surface of cooling joints formed at about 750 °C. At this temperature, a residual and immiscible fluid, rich in copper, migrated along joints depositing native copper coeval with lava solidification. The late magmatic model proposed by Szubert et al. (1979) invoked native copper deposition in microfractures and in the core of basaltic flows but also included a hydrothermal component. Pinto et al. (2011b) and Arena et al. (2014) favored the hydrothermal model based on the H1, H2, and H3 hydrothermal events.

Magmatic native copper crystallization occurs in equilibrium with the magma. Native copper formed at this condition is characterized by δ^{65}Cu values of about 0‰ and no significant fractionation (Markl et al. 2006). The isotopic compositions of WR mantle peridotite and basalt (Liu et al. 2015) as native copper crystals in ultramafic rocks (Albarède 2004; Ikehata and Hirata 2012) show δ^{65}Cu values between −0.15 and 0.2‰. These values support the absence of significant copper fractionation during magmatic, high-temperature processes. Thus, δ^{65}Cu values higher than 0.3‰ cannot be expected at high temperatures. Therefore, a magmatic origin of native copper can be excluded in the PVP because δ^{65}Cu values are between −0.9 and 1.9‰. Further evidence for a non-magmatic origin is as follows:

(1) Cabral and Beaudoin (2007) documented feldspar-hosted inclusions of native copper, ~50 μm in length, which were interpreted as magmatic in origin, in the Quebec Appalachians (Canada). Careful search for native copper inclusions in magmatic minerals of the host basalts of the PVP by backscattered-electron imaging did not yield inclusions.
(2) Cabral and Beaudoin (2007) compared the high-temperature native copper from Québec, Canada, and the low-temperature native copper deposits from the Keweenaw volcanic province, MI, in a S versus As diagram. High concentrations of sulfur (~10,000 ppm) and arsenic (~1000 ppm) characterize the high-temperature native copper from Québec, whereas only ~100 ppm S and 150 ppm As are detected in native copper from MI. The EPMA results for PVP native copper show sulfur contents close to, or below, the detection limit and As below the detection limit.
(3) Native copper along cooling joints in the PVP basalt acts as a time marker. Surface cracking, e.g., at Kilauea volcano, starts at 900 °C (Peck and Minakami 1968), but the cooling joint formation is completed when the bulk of the flow reaches around 750 °C (Lore et al. 2000), when the volcanic rock is consolidated. Native copper mineralization in the PVP occurs along cooling joints. This observation indicates that the cooling joints were formed prior to native copper. In addition, the occurrence of native copper in the host basalt is spatially associated with smectite. In cavities containing rounded massive copper, zeolite is found with and without calcite.

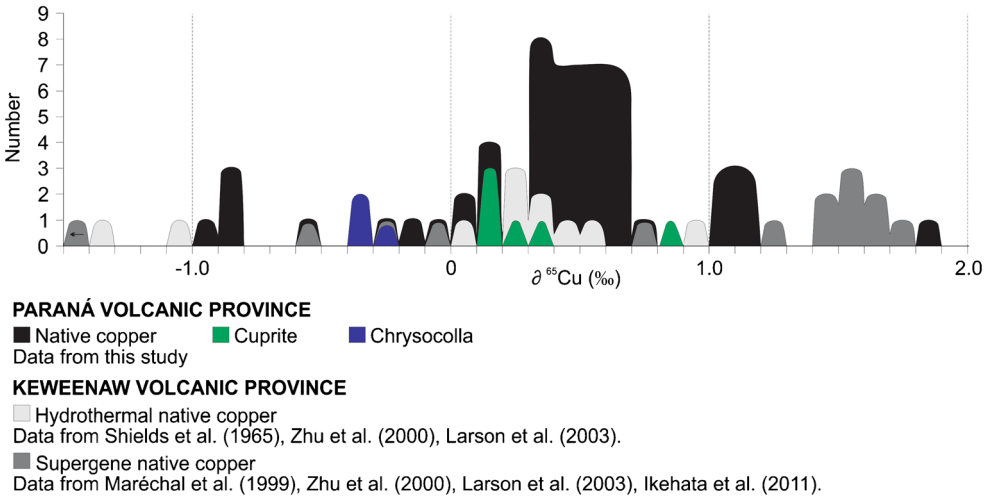

Fig. 11 Comparative histogram of δ^{65}Cu values of Paraná and Keweenaw volcanic provinces

According to the lines of evidence outlined above, the origin of native copper of the PVP is not compatible with magmatic processes. The Cretaceous native copper mineralization in the study area can be better compared with the Proterozoic native copper from the Keweenaw Province, USA (Fig. 11), and with the Upper Permian native copper from the Emeishan volcanic province in China. In the Keweenaw Province, native copper deposits are hosted in the top portion of rift-related, subaerial basaltic lava flows (Bornhorst and Barron 2011). Fluid inclusion studies (Livnat 1983) indicate that hydrothermal fluids at 150–200 °C penetrated the underlying conglomerates and the volcanic pile to deposit native copper at the top. In the Emeishan province, the host volcanic rocks, basalt, breccia, and tuff, containing bitumen and average Cu contents of 200 ppm, are interbedded with carbonaceous sedimentary rocks (Li et al. 2005). The Emeishan native copper mineralization is hosted in breccia, amygdaloidal crusts, and also in sedimentary rocks at the top of basalt flows. In places, native copper replaces and fills bituminous fissures in the basaltic rock, being spatially associated with a low-temperature assemblage of laumontite, epidote, and quartz. This assemblage points to an epigenetic hydrothermal mineralization (Li et al. 2005). In the PVP, the hydrothermal events (Hartmann 2008; Hartmann et al. 2012a, 2012b) were triggered by boiling water and its vapor from the Guarani aquifer. This water migrated upwards into the volcanic pile and promoted alteration in the host basalts, depositing zeolite and native copper in cooling joints, fractures, and cavities.

If a hydrothermal model is advanced for the PVP native copper, its metal source needs to be considered. In the MI district, this issue has been discussed for over a century. There, a possible source is the copper present in the crystal structure of iron minerals in the host basalt (e.g., Butler and Burbank 1929). The study performed by Cornwall (1956) determined copper in magnetite (200–800 ppm), ilmenite (90–300 ppm), clinopyroxene (51–320 ppm), and plagioclase (20–73 ppm). In the PVP, some studies have also suggested the presence of copper in magnetite (Tazaki et al. 1988; Arioli 2008; Pinto et al. 2011b).

Our LA-ICP-MS analyses show that basalt-forming minerals, mainly magnetite, contain significant amounts of copper. This finding contributes to a better understanding of the behavior of copper during the hydrothermal events. The Cretaceous hydrothermal alteration was caused by boiling Si-rich aqueous fluid from the Guarani aquifer. This event promoted chemical changes in the host basalt minerals (with release of copper) and formation of clay minerals (smectites). Studies involving basaltic rocks from other provinces describe the association of smectites in basalt (e.g., Yui and Chang 1999; Meunier 2005; Greenberger et al. 2012), and the alteration reaction triggered in the basalt minerals to form smectite (e.g., Xu et al. 1997; Meunier 2005).

In the PVP, smectites play an important role in the occurrence of native copper. The hydrothermal fluids leached the copper and promoted a first concentration in smectite (Fig. 10). As the hydrothermal activity developed, copper was deposited along the cooling joints that served as pathways for hydrothermal fluids. Similarly, the copper mineralization was deposited in cavities in the amygdaloidal crusts. Studies in monophase fluid inclusions in amethyst deposits (Gilg et al. 2003; Duarte et al. 2009; Morteani et al. 2010; Juchem 2014) showed

that the evolved boiling fluids had low salinity and temperatures up to 150 °C, although Gilg et al. (2014) determined the additional presence of high-salinity fluids. The presence of heulandite, identified by Raman spectroscopy, and calcite means that the copper mineralogical association formed at temperatures lower than 200 °C (Carr et al. 1999). These temperatures are consistent with those (100–150 °C) indicated by Pinto et al. (2011b) for the copper mineralization in the Vista Alegre mining district of the PVP and also for the hydrothermal alteration assemblage of smectite, zeolite, quartz, and calcite.

The formation of copper deposits includes Cu isotope fractionation mechanisms that are not fully understood. Several studies suggest that Cu isotope fractionation mechanisms are influenced by redox reactions, valence of copper ions, speciation in solution, and, in some cases, organic compounds (Zhu et al. 2000; Larson et al. 2003; Markl et al. 2006). In hydrothermal deposits, the most significant mechanisms are liquid–vapor separation, multi-step equilibrium processes, and physical/chemical parameters (temperature, oxygen fugacity, pH, and salinity of the fluid), which can be used to define the origin of the Cu deposits (Maréchal et al. 1999; Dekov et al. 2013; Zhang et al. 2013) and also to distinguish high- from low-temperature processes (Larson et al. 2003; Seo et al. 2007; Mathur et al. 2009, 2012). The Cu isotope fractionation in hydrothermal systems (Graham et al. 2004) in sulfides is associated with the ore-bearing fluid and the process of Cu leaching. In basalt-hosted hydrothermal Cu deposits, the copper isotopic values are similar to the mantle (~0‰, Larson et al. 2003; ~0.06‰, Liu et al. 2015) but may overlap those for chalcopyrite with values ranging between −1.5 and ~1.3‰ (Larson et al. 2003).

In the supergene environment, repetitive fractionation processes, during leaching, oxidation, and reduction, which are controlled by changes in the water system over time (Maher, 2005) cause strong Cu isotope fractionation (Larson et al. 2003; Maher 2005; Markl et al. 2006; Mathur et al. 2012). Large fractionation (9‰) may reflect an open system or kinetic effect (Sherman 2013). The δ^{65}Cu of supergene deposits involves three processes, leaching of copper from existing minerals, change in the valence of copper, and precipitation of copper minerals (Maher, 2005). The degree of leaching of the heavier ^{65}Cu isotope in the copper precursor mineral defines the final isotope ratio of the deposit. Supergene copper minerals co-existing in the same sample can be isotopically heavier than the precursor mineral (Asael et al. 2007), but the low-temperature fractionation can precipitate minerals isotopically lighter than the fluid (Maréchal and Sheppard, 2002). The supergene enrichment results in oxidized secondary phases (e.g., cuprite) with isotopic ratios higher than that of native copper. The δ^{65}Cu variations in supergene native copper deposits range from −3.03‰ (Maréchal et al. 1999) to 0.72‰ (Larson et al. 2003) and up to 1.8‰ (Ikehata et al. 2011). These variations overlap the isotope ratios from the MI native copper hydrothermal deposits (Shields et al. 1965; Larson et al. 2003; Maher 2005).

In the PVP, the hydrothermal fluids (water and its vapor) generated widespread native copper mineralization. The variation of δ^{65}Cu in the native copper is interpreted as isotopic fractionation reactions during low-temperature hydrothermal events followed by supergene alteration. The succession of hydrothermal events, followed by the redox reactions in the exposed volcanic flows at the surface, ensured the formation of the secondary co-existing copper minerals with native copper as precursor mineral.

The isotopic analyses of native copper crystals from Dom Pedro de Alcântara (RS) presented two different δ^{65}Cu values. In specimen FS86a, negative isotopic values (−0.59 to −0.91‰) were obtained, while in specimen FS86b the isotopic ratios are 0.02 and 0.09‰, indicating at least two different hydrothermal mineralization events and in the case of FS86a the leaching of the lighter δ^{65}Cu values. Similarly, in specimen JS4 (Santo Augusto region), the isotope ratios of 0.69 and 1.07‰ show two different fractionation events for Cu isotopes during the hydrothermal copper mineralization. Cuprite from this same specimen shows an isotope variation in the core (~0.18‰) with more fractionated δ^{65}Cu (up to 0.73‰) in the rim (Table 2).

The identification of different δ^{65}Cu ratios in native copper crystals was also made in specimen PD1 from Taquaruçu do Sul (PD1a = 0.71‰ and PD1b = 1.18‰) and, near PVP depocenter, in specimen CP14 from Cascavel (CP14a = 0.62‰ and CP14b = 1.89‰). In these cases, the variations of the isotopic ratios are restricted to positive values, indicating distinct hydrothermal mineralization events and fractionation along the fluid flow pathways at different times.

Supergene environment in the PVP promoted varied degrees of leaching and fractionation of Cu isotopes. Isotope analyses in the native dendritic copper W247 from Frederico Westphalen show substantial variations from the core (0.37‰) to the rim (−0.05 to −0.20‰), while in the region of Francisco Beltrão the specimen P1C showed a subtle variation (mean) from core (~0.40‰) to rim (~0.36‰).

Accordingly, the origin of native copper in the PVP is hydrothermal. The occurrences of native copper were generated by multiple hydrothermal pulses during the Cretaceous low-temperature hydrothermal events.

Conclusions

Hydrothermal native copper mineralization is widespread in the PVP as dendrites and needles in cooling joints, fractures, and also as filling of cavities in amygdaloidal crusts. Native copper, cuprite, tenorite, chrysocolla, malachite, and azurite make up the copper mineralization.

The origin of copper in the PVP is associated with the ascent of magma from the mantle to the surface and its extrusion as basaltic flows. Copper is present as a trace element in basalt-forming minerals, mainly in magnetite, explaining the average copper content of ~200 ppm in the host basalt. The Cretaceous hydrothermal events altered the volcanic rocks, so the magmatic magnetite, ilmenite, clinopyroxene, and the microcrystalline matrix were altered to smectite. Copper and silver were released from igneous minerals. Copper was partly concentrated in smectite. The δ^{65}Cu values in the PVP reflect the isotopic fractionation reactions during low-temperature hydrothermal and supergene events. The native copper mineralization occurred in pulses according to the evolution of the hydrothermal events. The secondary copper minerals formed by redox reactions in a supergene environment, with native copper as precursor mineral.

Acknowledgements The financial support was provided by Project VALE/CNPq, MCT, and Mineral Sector Fund (CT-Mineral) entitled "Desenvolvimento de metodologia de exploração geológica para geodos de ametista e ágata, cobre e outros bens minerais em ambiente hidrotermal do Grupo Serra Geral, sul-sudeste do Brasil" and project of excellence PRONEX-FAPERGS/CNPq on strategic minerals from southern Brazil, coordinated by Léo A. Hartmann. The authors wish to thank P.C. Soares, A.R. Cabral, three anonymous reviewers and the editors Frank Melcher and Georges Beaudoin for their comments that helped to improve the manuscript.

References

Albarède F (2004) The stable isotope geochemistry of copper and zinc. Rev Mineral Geochem 55:409–427

Almeida FFM (1986) Distribuição regional e relações tectônicas do magmatismo pós-paleozóico no Brasil. Rev Bras Geociências 16: 325–349

Arena KR, Hartmann LA, Baggio SB (2014) Geological controls of copper, gold and silver in the Serra Geral Group, Realeza region, Paraná, Brazil. Ore Geol Rev 63:178–200

Arioli EE (2008) Arquitetura faciológica da sequência vulcânica e o significado exploratório das anomalias geoquímicas de elementos do grupo da platina (EGP) e metais associados no sistema magmático Serra Geral, Estado do Paraná, Brasil. PhD Thesis, Universidade Federal do Paraná, Curitiba, Brazil, 262 p.

Asael D, Matthews A, Bar-Matthews M, Halicz L (2007) Copper isotope fractionation in sedimentary copper mineralization (Timna Valley, Israel). Chem Geol 243:238–254

Bellieni G, Comin-Chiaramonti P, Marques LS, Melfi AJ, Piccirillo EM, Nardy AJ, Roisenberg A (1984) High- and low-Ti flood basalts from the Paraná Plateau (Brazil): petrology and geochemical aspects bearing on their mantle origin. Neues Jahrb Mineral Abh 150:272–306

Bornhorst TJ, Barron RJ (2011) Copper deposits of the western Upper Peninsula of Michigan. Geol Soc Am 24:83–99

Butler BS, Burbank WS (1929) The copper deposits of Michigan. U.S. Government printing office, 238pp. Washington

Cabral AR, Beaudoin G (2007) Volcanic red-bed copper mineralization related to submarine basalt alteration, Mont Alexandre, Quebec Appalachians, Canada. Mineral Deposita 42:901–912

Carr PF, Pemberton JW, Nunan E (1999) Low-grade metamorphism of mafic lavas, upper Permian Broughton Formation, Sydney Basin. Aust J Earth Sci 46:839–849

Cornwall HR (1956) A summary of ideas on the origin of native copper deposits. Econ Geol 51:615–631

Costa AFU (1982) Geologia aplicada à prospecção de cobre em basaltos na área de Vista Alegre: Frederico Westphalen, RS. Acta Geol Leopold 11:17–36

Dekov VM, Rouxel O, Asael D, Hålenius U, Munnik F (2013) Native Cu from the oceanic crust: isotopic insights into native metal origin. Chem Geol 359:136–149

Duarte LC, Hartmann LA, Vasconcelos MAS, Medeiros JTN, Theye T (2009) Epigenetic formation of amethyst-bearing geodes from Los Catalanes gemological district, Artigas, Uruguay, southern Paraná Magmatic Province. J Volcanol Geoth Res 184:427–436

Duarte LC, Hartmann LA, Ronchi LH, Berner Z, Theye T, Massonne HJ (2011) Stable isotope and mineralogical investigation of the genesis of amethyst geodes in the los Catalanes gemological district, Uruguay, southernmost Paraná volcanic province. Mineral Deposita 46:239–255

Frank HT, Gomes MEB, Formoso ML (2009) Review of the areal extent and the volume of the Serra Geral Formation, Paraná Basin, South America. Pesquisas em Geociências UFRGS 36:49–57

Gilg HA, Morteani G, Kostitsyn Y, Preinfalk C, Gatter I, Strieder AJ (2003) Genesis of amethyst geodes in basaltic rocks of the rocks of the Serra Geral Formation (Ametista do Sul, Rio Grande do Sul, Brazil): a fluid inclusion, REE, oxygen, carbon and Sr isotope study on basalt, quartz, and calcite. Mineral Deposita 38:1009–1025

Gilg HA, Krüger Y, Taubald H, van der Kerkhof AM, Frenz M, Morteani G (2014) Mineralisation of amethyst-bearing geodes in Ametista do Sul (Brazil) from low-temperature sedimentary brines: evidence from monophase liquid inclusions and stable isotopes. Mineral Deposita 49:861–877

Gordon Jr M (1947) Classification of the Gondwanic rocks of Paraná, Santa Catarina and Rio Grande do Sul. Rio de Janeiro: DNPM, Divisão de Geologia e Mineralogia, Notas Preliminares e Estudos 38a:1–19

Graham S, Pearson N, Jackson S, Griffin W, O'Reilly S (2004) Tracing Cu and Fe from source to porphyry: in situ determination of Cu and Fe isotope ratios in sulfides from the Grasberg Cu-Au deposit. Chem Geol 207:147–169

Greenberger RN, Mustard JF, Kumar PS, Dyar MD, Breves EA, Sklute EC (2012) Low temperature aqueous alteration of basalt: mineral

assemblages of Deccan basalts and implication for Mars. J Geophys Res 117:E00J12

Hartmann LA (2008) Amethyst geodes formed from hot water in dinosaur times, 1st edn. UFRGS, Porto Alegre **57 pp**

Hartmann LA, Wildner W, Duarte LC, Duarte SK, Pertille J, Arena KR, Martins LC, Dias N.L (2010) Geochemical and scintillometric characterization and correlation of amethyst-bearing Paraná lavas from the Quaraí and Los Catalanes districts, Brazil and Uruguay. Geol Mag 147:954–970

Hartmann LA, Duarte LC, Massonne HJ, Michelin C, Rosenstengel LM, Bergmann M, Theye T, Pertille J, Arena KR, Duarte SK, Pinto VM, Barboza EG, Rosa MLCC, Wildner W (2012a) Sequential opening and filling of cavities forming vesicles, amygdales and giant amethyst geodes in lavas from the southern Paraná volcanic province, Brazil and Uruguay. Int Geol Rev 54:1–14

Hartmann LA, Medeiros JTN, Petruzzellis LT (2012b) Numerical simulations of amethyst geode cavity formation by ballooning of altered Paraná volcanic rocks, South America. Geofluids 12:133–141

Horn I, von Blanckenburg F (2007) Investigation on elemental and isotopic fractionation during 196 nm femtosecond laser ablation multiple collector inductively coupled plasma mass spectrometry. Spectrochim Acta B 62:410–422

Horn I, von Blanckenburg F, Schoenberg R, Steinhoefel G, Markl G (2006) In situ iron isotope ratio determination using UV-femtosecond laser ablation with application to hydrothermal ore formation processes. Geochim Cosmochim Acta 70:3677–3688

Hussak E (1906) Ueber das Vorkommen von gediegen Kupfer in den Diabasen von São Paulo. Centralb Mineral, pp 333–335

Ikehata K, Hirata T (2012) Copper isotope characteristics of copper-rich minerals from the Horoman peridotite complex, Hokkaido, northern Japan. Econ Geol 107:1489–1497

Ikehata K, Notsu K, Hirata T (2011) Copper isotope characteristics of copper-rich minerals from Besshi-type volcanogenic massive sulfide deposits, Japan, determined using a femtosecond LA-MC-ICP-MS. Econ Geol 106:307–316

Janasi VA, Freitas VA, Heaman LH (2011) The onset of flood basalt volcanism, Northern Paraná Basin, Brazil: a precise U Pb baddeleyite/zircon age for a Chapecó-type dacite. Earth Planet Sci Lett 302:147–153

Juchem PL (2014) Amethyst mineralization in rhyodacites of the Serra Geral Group, Paraná volcanic Province. In: Hartmann LA, Baggio SB (orgs) Metallogeny and mineral exploration in the Serra Geral Group, 1st ed. UFRGS, Porto Alegre, pp 321–334

Larson PB, Maher K, Ramos FC, Chang Z, Gaspar M, Meinert LD (2003) Copper isotope ratios in magmatic and hydrothermal ore-forming environments. Chem Geol 201:337–350

Lazarov M, Horn I (2015) Matrix and energy effects during in situ determinations of Cu isotope ratios by UV-femtosecond laser ablation multicollector inductively coupled plasma mass spectrometry. Spectrochim Acta B 111:64–73

Le Bas MJ, Le Maitre RW, Streckeisen A, Zanettin B (1986) A chemical classification of volcanic-rocks based on the total alkali sílica diagram. J Petrol 3:745–750

Li H, Mao J, Chen Y, Wang D, Zhang C, Xu H (2005) Epigenetic hydrothermal features of the Emeishan basalt copper mineralization in NE Yunnan, SW China. In: Mao J, Bierlein FP (eds) Mineral deposit research: meeting the global challenge. Springer Berlin Heidelberg, Beijing, pp 149–152

Liu S-A, Huang J, Liu J, Wörner G, Yang W, Tang Y-J, Chen Y, Tang L, Zheng J, Li S (2015) Copper isotopic composition of the silicate Earth. Earth Planet Sc Lett 427:95–103

Livnat A (1983) Metamorphism and copper mineralization of the Portage Lake Lava Series, northern Michigan. PhD Thesis, University of Michigan, Ann Arbor, USA

Lore J, Gao H, Aydin A (2000) Viscoelastic thermal stress in cooling basalt flows. J Geophys Res 105:695–709

Maher KC (2005) Analysis of copper isotope ratios by multi-collector inductively coupled plasma mass spectrometry and interpretation of copper isotope ratios from copper mineralization. PhD Thesis, Washington State University, USA, 239 pp

Mantovani MSM, Marques LS, De Sousa MA, Civetta L, Atalla L, Innocenti F (1985) Trace element and strontium isotope constraints on the origin and evolution of Paraná continental flood basalts of Santa Catarina state (southern Brazil). J Petrol 26:187–209

Maréchal C, Sheppard SMF (2002) Isotopic fractionation of Cu and Zn between chloride and nitrate solutions and malachite or smithsonite at 30° and 50° C. Geochim Cosmochim Acta 66:A484

Maréchal C, Télouk P, Albarède F (1999) Precise analysis of copper and zinc isotopic compositions by plasma-source mass spectrometry. Chem Geol 156:251–273

Markl G, Lahaye Y, Schwinn G (2006) Copper isotopes as monitors of redox processes in hydrothermal mineralization. Geochim Cosmochim Acta 70:4215–4228

Massonne HJ, Opitz J, Theye T, Nasir S (2013) Evolution of a very deeply subducted metasediment from As Sifah, northeastern coast of Oman. Lithos 156 – 159:171–185

Mathur R, Titley S, Barra F, Brantley S, Wilson M, Phillips A, Munizaga F, Maksaev V, Vervoort J, Hart G (2009) Exploration potential of cu isotope fractionation in porphyry copper deposits. J Geochem Explor 102:1–6

Mathur R, Ruiz J, Casselman MJ, Megaw P, Van Egmond R (2012) Use of Cu isotopes to distinguish primary and secondary Cu mineralization in the Cañarico Norte porphyry copper deposit, Northern Peru. Mineral Deposita 47:755–762

Melfi AJ, Piccirillo EM, Nardy AJR (1988) Geological and magmatic aspects of the Paraná Basin an introduction. In: Piccirillo EM, Melfi AJ (eds) The Mesozoic flood volcanism of the Paraná Basin: Petrogenetic and geophysical aspects. IAG, USP, São Paulo, pp 1–13

Mello SK (2000) Estudo petrológico da região de Água Perdida no vale do Rio Piquiri – PR: Reconhecimento das mineralizações de cobre e produtos de alteração em rochas básicas da Formação Serra Geral – Bacia do Paraná. PPGeo UNISINOS, São Leopoldo, Brazil

Meunier A (2005) Clays. Springer Berlin Heidelberg, New York **472 p**

Morteani G, Kostitsyn Y, Preinfalk C, Gilg HA (2010) The genesis of the amethyst geodes at Artigas (Uruguay) and the paleohydrology of the Guarani aquifer: structural, geochemical, oxygen, carbon, strontium isotope and fluid inclusion study. Int J Earth Sci 99: 927–947

Nakamura K, Wildner W, Shibuya A, Masuta K, Murakami T, Romanini S (2003) Mineral exploration of the Cu–Ni PGE deposits in the Paraná Basin, Southern Brazil, phase II. Tokyo, Japan Mining Engineering Center for International Cooperation–JMEC/ Geological Survey of Brazil–CPRM, Porto Alegre, Brazil

Oeser M, Weyer S, Horn I, Schuth S (2014) High-precision Fe and Mg isotope ratios of silicate reference glasses determined in situ by femtosecond LA-MC-ICP-MS and by solution nebulisation MC-ICP-MS. Geostand Geoanal Res 38:311–328

Peate DW (1997) The Paraná-Etendeka Province. In: Mahoney JJ, Coffin MR (eds) Large igneous provinces: continental, oceanic, and planetary flood volcanism, Geophysical Monograph Series, vol vol 100. American Geophysical Union, Washington DC, pp 217–245

Peate DW, Hawkesworth CJ, Mantovani MSM (1992) Chemical stratigraphy of the Paraná lavas (South America): classification of magma types and their spatial distribution. Bull Volcanol 55:119–139

Peate DW, Hawkesworth CJ, Mantovani MSM, Rogers NW, Turner SP (1999) Petrogenesis and stratigraphy of the high-Ti/Y Urubuci magma type in the Paraná flood basalt province and implications for the nature of 'Dupal'-type mantle in the south Atlantic region. J Petrol 40:451–473

Peck DL, Minakami T (1968) Formation of columnar joints in the upper part of Kilauean lava lakes, Hawaii. Bull Geol Soc Am 79:1151–1166

Pinto VM, Hartmann LA (2011) Flow-by-flow chemical stratigraphy and evolution of thirteen Serra Geral Group basalt flows from Vista Alegre, southernmost Brazil. An Acad Bras Ciênc 83:425–440

Pinto VM, Hartmann LA, Santos JOS, McNaughton NJ, Wildner W (2011a) Zircon U–Pb geochronology from the Paraná bimodal volcanic province support a brief eruptive cycle at 135 Ma. Chem Geol 281:93–102

Pinto VM, Hartmann LA, Wildner W (2011b) Epigenetic hydrothermal origin of native copper and supergene enrichment in the Vista Alegre district, Paraná basaltic province, southernmost Brazil. Int Geol Rev 53:1163–1179

Rosenstengel LM, Hartmann LA (2012) Geochemical stratigraphy of lavas and fault-block structures in the Ametista do Sul geode mining district, Paraná volcanic province, southern Brazil. Ore Geol Rev 48: 332–348

Seo JH, Lee SK, Lee I (2007) Quantum chemical calculations of equilibrium copper (I) isotope fractionations in ore-forming fluids. Chem Geol 243:225–237

Sherman DM (2013) Equilibrium isotopic fractionation of copper during oxidation/reduction, aqueous complexation and ore-forming processes: predictions from hybrid density functional theory. Geochim Cosmochim Acta 118:85–97

Shields WR, Goldich SS, Garner EL, Murphy TJ (1965) Natural variations in the abundance ratio and the atomic weight of copper. J Geophys Res 70:479–491

Szubert EC, Grazia CA, Shintaku I (1979) Projeto Cobre em Itapiranga. CPRM SUREG, Porto Alegre **474 pp**

Tazaki K, Fyfe WS, Tazaki K, Bischoff J, Rocha BR (1988) Occurrence of copper films in basalt from the Serra Geral formation, Paraná Basin, Brazil. Rev Bras Geoc 18:332–337

White C (1908) Relatório Final. Comissão de Estudos das Minas de Carvão de Pedra do Brazil. Imprensa Nacional, Rio de Janeiro. Re-impressão - Edição Comemorativa: 100 anos do Relatório White, CPRM, 2008, Belo Horizonte, 617 pp

Wildner W, Hartmann LA, Cunha-Lopes R (2009) A proposed stratigraphy for the Serra Geral Group in the Paraná Basin. In: Milani EJ, Chemale F Jr (eds) Correlation Brazil–Africa. PETROBRAS, Gramado

Xu W, Van der Voo R, Peacor DR, Beaubouef RT (1997) Alteration and dissolution of fine-grained magnetite and its effects on magnetization of the ocean floor. Earth Planet Sci Lett 151:279–288

Yui TF, Chang SS (1999) Formation conditions of vesicle/fissure-filling smectites in Penghu basalts: a stable-isotope assessment. Clay Miner 34:381–393

Zhang D, Zhou T, Yuan F, Fiorentini ML, Said N, Lu Y, Pirajno F (2013) Geochemical and isotopic constraints on the genesis of the Jueluotage native copper mineralized basalt, Eastern Tianshan, Northwest China. J Asian Earth Sci 73:317–333

Zhu XK, O'Nions RK, Guo Y, Belshaw NS, Rickard D (2000) Determination of natural Cu-isotope variation by plasma-source mass spectrometry: implications for use as geochemical tracers. Chem Geol 163:139–149